INSTITUTE OF PHYSICS PUBLISHING JOURNAL OF PHYSICS: CONDENSED MATTER

J. Phys.: Condens. Matter **15** (2003) R1641–R1667 PII: S0953-8984(03)58996-2

TOPICAL REVIEW

Photoionization spectroscopy of deep defects responsible for current collapse in nitride-based field effect transistors

P B Klein and S C Binari

Naval Research Laboratory, Washington, DC 20375, USA

Received 1 September 2003
Published 24 October 2003
Online at stacks.iop.org/JPhysCM/15/R1641

Abstract

This review is concerned with the characterization and identification of the deep centres that cause current collapse in nitride-based field effect transistors. Photoionization spectroscopy is an optical technique that has been developed to probe the characteristics of these defects. Measured spectral dependences provide information on trap depth, lattice coupling and on the location of the defects in the device structure. The spectrum of an individual trap may also be regarded as a 'fingerprint' of the defect, allowing the trap to be followed in response to the variation of external parameters. The basis for these measurements is derived through a modelling procedure that accounts quantitatively for the light-induced drain current increase in the collapsed device. Applying the model to fit the measured variation of drain current increase with light illumination provides an estimate of the concentrations and photoionization cross-sections of the deep defects. The results of photoionization studies of GaN metal–semiconductor field effect transistors and AlGaN/GaN high electron mobility transistors (HEMTs) grown by metal–organic chemical vapour deposition (MOCVD) are presented and the conclusions regarding the nature of the deep traps responsible are discussed. Finally, recent photoionization studies of current collapse induced by short-term (several hours) bias stress in AlGaN/GaN HEMTs are described and analysed for devices grown by both MOCVD and molecular beam epitaxy.

Contents

1. Introduction

There is great current interest in the development of nitride-based field effect transistors (FETs) for high power microwave applications. The AlGaN/GaN material system offers great potential for fabricating electronic device structures that operate at high temperature, high power, high frequency and in adverse environments [1]. This potential is the result of an advantageous combination of material properties, including a high critical breakdown field, good thermal conductivity, high peak and saturated electron velocities, a large bandgap and the ability to form high quality hetero-interfaces that produce a two-dimensional electron gas (2DEG) with high sheet charge density ($\approx 10^{13}$ cm^{-2}). Consequently, excellent device characteristics (e.g. 9.8 W mm^{-1} at 8 GHz [2]) have been reported for AlGaN/GaN high electron mobility transistors (HEMTs).

There are, however, a number of difficulties to be overcome before nitride devices can become available for mainstream applications. While great strides have been made in the growth of high quality nitride materials, further development in this area is necessary in order to provide wafers that are reproducible and of low defect density. In addition, there is currently no source of large-area bulk GaN substrates. As a result, nitride epitaxial layers are generally grown on SiC or sapphire wafers. The substantial mismatch in lattice constant and thermal conductivity between the substrate and epitaxial layer results in significant biaxial strain and a high concentration of extended defects. Impurities or lattice defects can also be incorporated during epitaxial growth. Additionally, impurities can decorate the extended defects. Any of these defect sites can be electrically active and can therefore contribute to trapping and recombination within the device structure, leading to a degradation in the output characteristics of the device. The role of traps in limiting the performance of nitride-based FETs has been reviewed recently by Binari *et al* [3].

Two phenomena that limit the achievable output power of nitride-based FETs are RF dispersion and current collapse. In RF dispersion, the device output power measured at high frequency (typically several gigahertz) is found to be substantially reduced from that projected from the dc I–V characteristics. This effect has been associated [4, 5] with the trapping of charge on the surface. In contrast, current collapse is a reduction in the dc drain current and a distortion of the dc I–V characteristic that occurs when a large drain–source voltage is applied to the device. The collapse generally results from the trapping of channel carriers by deep defects within the device structure. This phenomenon is specifically associated with deep centres, since carriers trapped at shallow defects/impurities are rapidly re-emitted at the operating temperatures of typical devices.

It has become common in the recent literature to refer to RF dispersion as either 'RF current collapse' or simply 'current collapse'. This unfortunate choice of terminology has led to some real confusion, as characteristics of one effect have been attributed to the other. While

they both contribute to a loss in FET output power, current collapse and RF dispersion arise from very different mechanisms and operate in very different frequency regimes (i.e. dc versus high frequency). In this review, we will concentrate specifically on effects related to current collapse.

In order to mitigate or eliminate the effects of current collapse, it is essential to gain some understanding of the nature of the defects that are responsible for this effect. Recently, an optical technique, photoionization spectroscopy, has been developed [6–8] specifically to probe these trapping centres. By measuring the optical absorption spectrum associated with the photoionization process that releases the trapped carriers, photoionization spectroscopy provides a method for identifying the unique spectral signature associated with each defect responsible for the collapse and a means for acquiring information about the concentrations, photoionization cross-sections, locations and chemical identities of the defects involved. In this review, we will provide an overview of current collapse in FET structures and a detailed description of photoionization spectroscopy and the analytical models that are employed to interpret the data. Photoionization studies of GaN MESFETs and AlGaN/GaN HEMTs grown by either metal–organic chemical vapour deposition (MOCVD) or molecular beam epitaxy (MBE) will be described and the implications regarding the defects responsible for the collapse will be discussed. Finally, recent photoionization studies of collapse induced by drain bias stress will be presented and compared to those of conventional current collapse.

2. Current collapse

Current collapse is a hot-carrier effect that is most often observed in small device structures where high applied electric fields are common. Carriers accelerated by the high field can gain sufficient kinetic energy to overcome local potential barriers and escape the high mobility channel. These carriers are then injected into a neighbouring region of the device that may contain a substantial concentration of deep trapping centres. Under these circumstances, the injected carriers can become trapped and can remain trapped after the high voltage is removed if the trapping centres are deep. When this occurs, the real space transfer of charge out of the conducting channel leads to the formation of a depletion region in the channel of a MESFET or the reduction of sheet charge in the case of a HEMT structure. The result in both cases is current collapse: a reduction in the drain current resulting from the application of a high drain–source voltage. It should be recognized that, in a collapsed device, the trapped carriers represent a *nonequilibrium* charge distribution: deep centres that are capable of trapping carriers during collapse must be empty in equilibrium and become filled by trapping injected hot carriers. When these carriers escape the deep traps, they return to equilibrium by drifting back to the conducting channel under the influence of the electric field that was created as a result of the original transfer of charge.

The observation of current collapse dates back at least twenty-five years, when distortions in the I–V characteristics were observed at high applied drain voltages for Si metal–oxide–semiconductor FETs (MOSFETs) [9, 10] and CdSe thin film transistors [11, 12]. In both cases, it was determined that injected carrier trapping at defects in the oxide layer was responsible for the collapse. The first use of the term ‘current collapse’ seems to have been by Fischer *et al* [13] in a study of collapse in AlGaAs/GaAs modulation-doped FETs (MODFETs) at cryogenic temperatures. Detailed studies concluded [14, 15] that the effect was the result of hot carrier injection into the AlGaAs layer, and that carriers were being trapped by the well-known DX centre. Current collapse could only be observed in the AlGaAs system at low temperature ($<$130 K). At higher temperatures the thermal energy of the trapped carriers was sufficient to overcome the barrier for emission from the DX centre, so that the carriers were rapidly re-emitted. Consequently, normal I–V characteristics could be restored by heating the device

above 130 K or by light illumination. This illustrates an important characteristic of current collapse in all systems—any excitation (e.g. thermal, optical) that is sufficient to release the trapped carriers will tend to restore the drain current. It is clear, therefore, that any deep defect that participates effectively in producing collapse must have an emission barrier that is large compared to kT. It is not uncommon that these centres will often have a large barrier to carrier capture as well. As in the case of the DX centre, such defects are then able to participate in persistent photoconductivity as well as current collapse.

It is also noteworthy that Kastalsky and Kiehl [16] proposed an alternative mechanism for current collapse in the AlGaAs/GaAs MODFET, in which hot carriers *in the doped AlGaAs layer* are accelerated in the region between gate and drain where the electric field is the greatest. These carriers gain enough kinetic energy to overcome the large DX centre capture barrier and become trapped. This leads to a region in the AlGaAs near the drain—*a high field domain*—where all of the carriers are trapped on DX centres. Due to the high ($\approx 2 \times 10^{18}$ cm^{-3}) concentration of DX centres, Kastalsky and Kiehl [16] concluded that a field-induced hopping transport within these domains leads to charge polarization within the domain region that results in the creation of a potential in the AlGaAs and GaAs channel that is responsible for current collapse. While this model is somewhat more complex than previous explanations for the collapse, it was successful in accounting for a wide range of behaviours in these device structures. In AlGaN/GaN HEMT structures, where the AlGaN layer is undoped and the 2DEG carriers result from the spontaneous and piezoelectric polarization in the wurtzite nitrides [17], this mechanism of collapse would be ineffective because of the lack of carriers in the AlGaN layer, independent of the existence of an appropriate defect. On the other hand, modulation doped AlGaN/GaN structures would be susceptible to this type of collapse, given the existence of a DX-type trapping centre. While such a defect has been observed and associated with oxygen in AlGaN ($x > 0.27$) [18], it was found to be stable only at low temperature (<150 K) and is not considered problematic for current AlGaN/GaN HEMT structures.

An example of the dramatic effect that a high applied drain voltage can have on the I–V characteristic of an AlGaN/GaN HEMT structure is shown in figure 1(a). These data, observed by Khan *et al* [19], represent the first report of current collapse in a nitride-based FET. The I–V s (i) and (ii), obtained before and after the application of a high drain bias, respectively, exhibit a very large decrease in channel conductance resulting from the high applied field. While the collapse observed in recent devices is not quite as complete as this (the collapsed device in figure 1(a) is essentially pinched off at low drain voltage), it is still sufficient to cause substantial reductions in FET output power.

The effect of collapse on the output power of an FET can be seen in the schematic I–V characteristics in figure 2, where the full and dotted curves represent the device I–V before and after collapse, respectively. The effect of the collapse is to increase the knee voltage and to decrease the maximum current. Both of these actions are seen to decrease the achievable output power, which is proportional to the product of the maximum current and voltage swings (ΔI, ΔV) about the quiescent point Q:

$$P_{\mathrm{MAX}} \cong \tfrac{1}{8} \Delta V \, \Delta I. \tag{1}$$

This product, representing the maximum achievable output power at low frequency, is reflected graphically in figure 2 as the area of the entire shaded region. Current collapse reduces this to the area of the broken rectangular region. In addition to reductions due to current collapse, as the frequency is increased, the achievable output power is further reduced by RF dispersion. This demonstrates the distinct roles played by RF dispersion and current collapse in limiting FET output power.

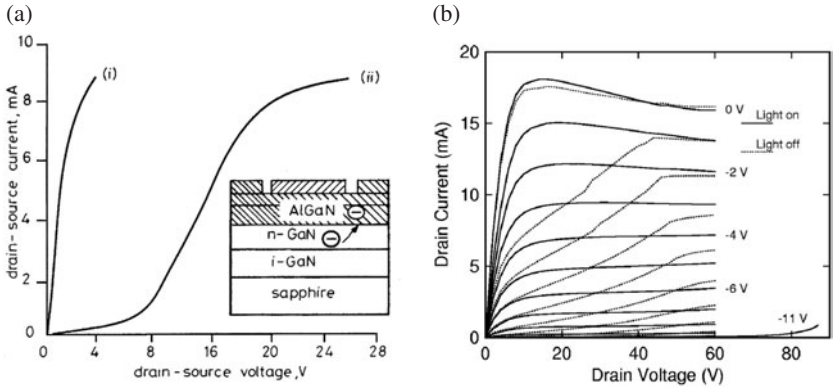

Figure 1. *I–V* characteristics exhibiting current collapse in (a) an AlGaN/GaN HEMT structure before (i) and after (ii) the application of a high drain bias (after [19]), and (b) a GaN MESFET, with (full curves) and without (dotted curves) light illumination (after [20]).

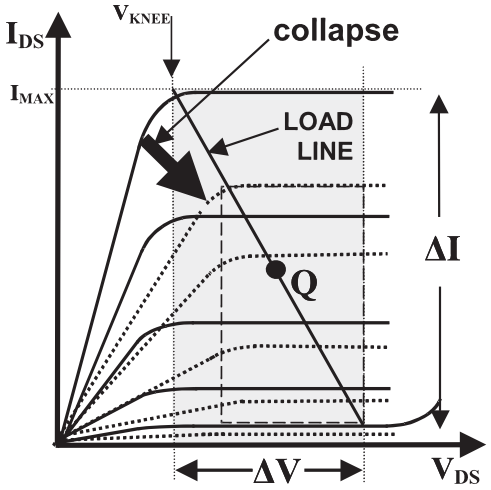

Figure 2. A sketch of FET *I–V* characteristics before (full curves) and after (dotted curves) current collapse. The maximum attainable device output power is approximately proportional to the area of the shaded and broken rectangles, before and after collapse, respectively.

Current collapse in a GaN MESFET was first reported by Binari *et al* [20]. The collapse is evident in comparing the *I–V* characteristics shown in figure 1(b): collapse is inhibited by light illumination for the full curves and is clearly present for the dotted curves measured in the dark. At elevated temperatures (up to 155 °C), the drain current exhibited little or no collapse, consistent with thermal emission from the deep traps, while the time dependence of the drain current recovery reflected a multi-component response, suggesting the involvement of multiple traps in the collapse. These results were interpreted in terms of deep traps in the high-resistivity (HR) MOCVD GaN buffer layer, which is grown under conditions that enhance trap formation in order to compensate for the shallow donors and produce HR material. Further studies [21, 22] confirmed the location of the traps in the HR GaN buffer layer: a wafer exhibiting variations in the conductivity of the HR GaN layer, between slightly conducting and HR, displayed collapse in those devices fabricated over the HR regions, while no collapse

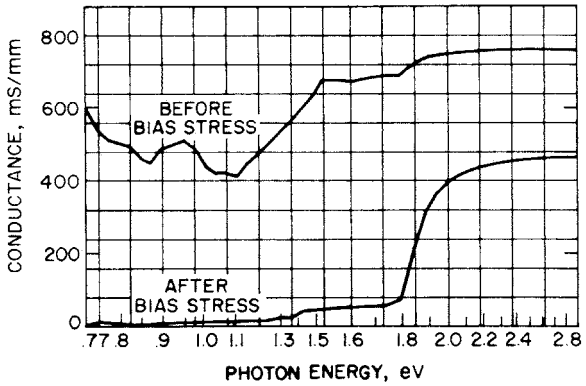

Figure 3. Effect of illumination wavelength on the conductance of an AlGaAs/GaAs HEMT structure before and after a large drain bias is applied. Current collapse is evident in the dramatic loss of conductance after a large bias is applied and is reversed when the incident photon energy exceeds the AlGaAs bandgap near 1.8 eV (after [16], ©1986 IEEE).

was observed from devices fabricated over the n-type regions. The traps in n-type GaN of these regions were already filled by compensating shallow donors.

Zhang *et al* [23] came to a similar conclusion in their study of high field effects in a GaN junction FET (JFET). The field-induced reduction in the drain current was interpreted as resulting from high-field injection and subsequent trapping of electrons in the HR GaN buffer layer near the drain side of the gate.

3. Photoionization spectroscopy

3.1. Overview

While the drain current recovery produced by illuminating a collapsed device with light has been understood from early on as resulting from the release of trapped carriers [12], there have been only a few attempts to investigate the spectral dependence of this effect. Kastalsky and Kiehl [16] followed the conductance of an AlGaAs/GaAs MODFET as the illumination wavelength was rapidly swept across the visible and near-infrared regions. A comparison of scans taken before and after the application of a high drain bias, indicated in figure 3, showed that the conductance of the device dropped by two orders of magnitude after the bias was applied (current collapse) and could be completely restored when the energy of the incident photons exceeded 1.8 eV—the AlGaAs bandgap. This was interpreted as confirmation that the traps responsible for the collapse were residing in the AlGaAs layer. Similarly, in their early study of AlGaN/GaN HEMTs, Khan *et al* [19] observed drain current restoration with light near the GaN bandgap, associated with the creation of free carriers, and near 650 nm (1.9 eV), which was attributed to the release of carriers by an unidentified trapping centre. Binari *et al* [20] studied the light-induced reversal of current collapse in GaN MESFETs by observing the restoration of the collapsed I–V curve as a function of the wavelength of the incident light. The observed monotonic increase in the efficacy of drain current restoration with increasing photon energy suggested that a broad, below-gap absorption process was associated with the traps. Photoionization spectroscopy developed from an effort to put these measurements on a more quantitative basis.

Photoionization spectroscopy is based on a simple idea: illuminating a collapsed device with light above the absorption threshold for releasing a trapped carrier from a deep defect

will lead to the de-trapping of the carrier and a corresponding increase in the drain current. During a photoionization spectroscopy measurement, the absorption is detected as a light-induced increase in the drain current above that of the fully collapsed device. As carriers are photoionized from the traps and drift back to the conducting channel, the filled trap concentration decreases and the drain current increases, roughly in proportion to the number of returning carriers. As described in section 4.2, this proportionality is valid only at low light levels and for measurements obtained within the linear part of the I–V characteristic.

The absorption spectrum associated with this photoionization process is a unique property of a given defect, with a well-defined absorption threshold energy, linewidth, absorption cross-section and lattice coupling. Consequently, this *photoionization spectrum* may be viewed as representative of the deep defect and may be employed to identify the defect in a manner similar to a photoluminescence band or a peak in a deep level transient spectroscopy (DLTS) measurement.

Obtaining the photoionization spectrum of a trap in a FET structure through direct optical absorption measurements would be difficult: for a trap with a reasonably large cross-section ($\approx 10^{-15}$ cm^2) and at a substantial concentration (10^{17} cm^{-3}), a 100 nm layer (i.e. $\approx 10^{12}$ cm^{-2}) would be expected to produce a change in transmission of only 0.1%, neglecting background absorption from the thick sapphire or SiC substrate. Photoionization spectroscopy provides a way to carry out this measurement with high sensitivity: absorptions corresponding to effective changes in transmission of $< 1 \times 10^{-6}$ have been measured [8]. The high sensitivity of this technique derives from the basic operating principle of a FET: small transfers of charge at the gate can control large variations in the drain current. Similarly, small quantities of trapped charge created under the gate by hot carrier injection can act as a 'virtual gate', leading to large reductions in the drain current.

Since the fully collapsed state corresponds to having all of the traps occupied that were initially filled by hot carrier injection, a natural measure of the light-induced *reversal* of current collapse is the fractional increase in the drain current, ΔI, above the collapsed drain current, I_{dark}. We therefore define [6] an optical response function $S(h\nu)$ to represent the increase in $\Delta I / I_{\text{dark}}$ per incident photon of energy $h\nu$:

$$S(h\nu) \equiv \frac{1}{\Phi_{h\nu} t} \frac{\Delta I(h\nu)}{I_{\text{dark}}}. \tag{2}$$

The total incident photon dose is $\Phi_{h\nu} t$(photons cm^{-2}), where $\Phi_{h\nu}$ is the incident photon flux and t is the illumination time. In order to translate the measured drain current increase, ΔI, into an optical cross-section, a definite model of the optically induced drain current recovery is required. The model described in section 4.2 will show that $S(h\nu)$ is proportional to the photoionization spectrum of the deep trap, if it is measured under the following conditions; (1) the light illumination is weak ($\sigma \Phi_{h\nu} t \ll 1$, where σ is the photoionization cross-section) and (2) the measurement of drain current increase is made at a drain voltage within the linear regime of the I–V characteristic. Consequently, all photoionization spectra are obtained under these conditions.

If monochromatic light of photon energy greater than the trap photoionization threshold illuminates a collapsed device, the drain current will begin to recover. For small doses of light, this increase in drain current is expected to vary linearly with light illumination. For large doses the drain current increase will eventually saturate, as all of the filled traps become emptied and the drain current returns to its pre-collapse value. It is clear that the saturation value of ΔI is related to the total number of traps that were emptied by the light. By employing the model that is developed in section 4.2 for drain current recovery, the measured dependence of drain current increase on total incident photon dose may be fitted to provide a determination

of the areal concentrations and photoionization cross-sections of the deep traps. These studies, referred to as *saturation measurements*, represent a technique that is complementary to the spectral dependence measurements and can provide valuable information about the deep traps responsible for current collapse.

3.2. Experimental implementation

In order to probe nitride-based devices optically, a broadly tunable light source in the range 250–1000 nm is necessary: a 75 W xenon lamp and a 0.22 m double grating spectrometer have been employed for this purpose in our laboratory. Using all-reflective optics and 1:1 imaging, this set-up delivers in the range of 100 μW at the peak of the lamp emission spectrum in a 14 mm^2 rectangular image and within a 3.5 nm bandpass. For spectral dependence measurements, the incident light must be kept weak enough so that the condition $\sigma\Phi_{h\nu}t \ll 1$ remains satisfied. In order to accomplish this, it is usually sufficient to attenuate the spectrometer output so that $\Delta I/I_{\mathrm{dark}}$ is no more than a few per cent.

Unless the device is wire-bonded, some form of probe station is necessary to contact the device of interest. In order to provide fixed and ramped bias voltages and to measure the resulting I–V curves, we have employed a Hewlett Packard model 4142B modular source/monitor under computer control. Prior to each measurement, it is useful to ensure that all of the traps are in their equilibrium state. This can be effected by illuminating the device with ionizing light for several seconds. For GaN, a blue GaN LED is convenient. Two consecutive I–V sweeps are then run with a measured delay between the sweeps (typically 10 s). Toward the end of the first sweep, the device experiences a large drain–source voltage and hot carriers escaping the conducting channel can be trapped in neighbouring regions of the device. At the end of this sweep, the device is in the collapsed state. During the delay between sweeps, the device can remain in the dark or it can be illuminated for the duration of the delay by the opening of a shutter. If the shutter remains closed, the second sweep exhibits an I–V representative of the collapsed state ($I_{\mathrm{d}s} = I_{\mathrm{dark}}$). When the measurement is repeated with the shutter open, the drain current increases above I_{dark} by ΔI. As noted above, the measurement of the drain current increase must be made at a drain voltage within the linear part of the I–V curve. Measuring closed-shutter sweeps both before and after the open-shutter sweeps was found effective in averaging out small drifts in the measurements, due primarily to the contacts. It is also necessary to make sure that the delay time between sweeps is small compared to the characteristic time for thermal emission of the trapped carriers, so that significant drain current recovery does not occur thermally before the collapsed state is probed by the second sweep.

Saturation measurements, in contrast to spectral dependence studies, are carried out at a single wavelength, which corresponds to a photon energy that is greater than the absorption threshold of at least one of the traps being investigated. The total photon dose is controlled by varying the incident light intensity, the illumination time or a combination of the two. The intensity can be controlled by employing a set of calibrated UV neutral density filters. While this is sufficient for most measurements, some of the saturation studies have required higher power at a fixed wavelength in order to empty all of the traps. In this case, it is necessary to use an attenuated laser source at the appropriate wavelength.

4. Photoionization spectroscopy in GaN MESFETs

4.1. Photoionization measurements

Photoionization spectroscopy was first reported [6] for a GaN MESFET. The resulting spectrum is shown as the open circles in figure 4(a). The device, consisting of a 200 nm thick channel

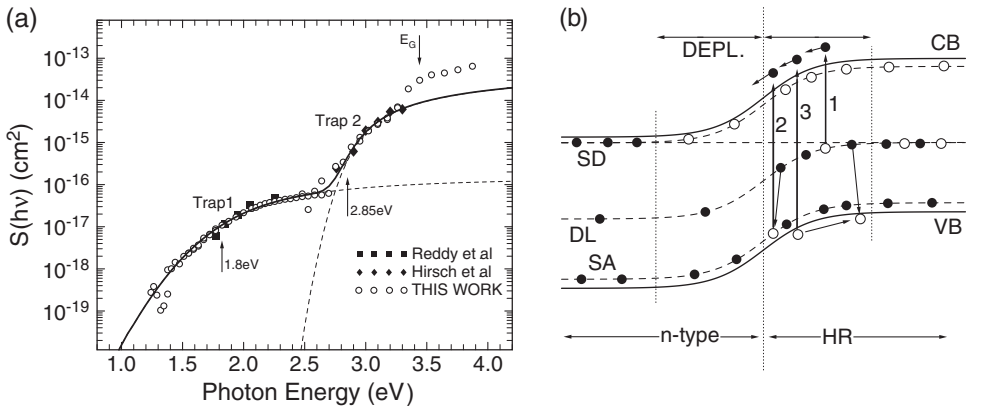

Figure 4. (a) Photoionization spectrum (open circles) of a GaN MESFET, indicating two broad absorption bands, Trap1 and Trap2, with ionization thresholds at 1.8 and 2.85 eV, respectively. The filled squares and diamonds are independent PPC spectra [31, 32]. (b) Sketch of the band structure of a collapsed GaN MESFET, with a positive depletion region in the n-GaN channel and a negatively charged region in the HR–GaN layer. The optical transitions 1, 2 and 3 create contributions to the spectrum in (a) due to deep traps, ionized shallow acceptors and photoexcited free carriers, respectively.

layer of n-GaN ($n \approx 2 \times 10^{17}$ cm^{-3}) on a 3 μm thick HR GaN buffer layer [20], was grown by MOCVD. The spectrum reflects the presence of two deep traps, represented by the two broad, below-gap absorption bands, which were labelled as Trap1 and Trap2. The spectral position of the two absorptions indicated that both traps were deep, while their breadth suggested that both were strongly coupled to the lattice. This was confirmed by the failure of common analytical forms [24, 25] to fit the measured spectral dependence of the absorption, while a good fit was obtained using an expression [26, 27] for the photoionization cross-section that takes lattice relaxation into account. The fitted curve (full curve in the figure), composed of the superposition of the two absorption bands (broken curves in the figure), corresponded to absorption threshold energies of 1.8 and 2.85 eV and Gaussian linewidths of 0.25 and 0.1 eV for Trap1 and Trap2, respectively.

The photoionization of electrons from the deep levels is indicated as transition '1' in the band diagram for the MESFET shown in figure 4(b). As indicated in the figure, the injection and trapping of hot channel carriers in the HR–GaN layer creates a positive depletion region in the n-type layer and a negatively charged region in the HR–GaN, where carriers are trapped at deep centres.

An additional threshold appears in the spectrum at about 3.2 eV, which, for room temperature GaN, corresponds to the energy to excite an electron from an ionized shallow acceptor to the conduction band, shown as transition '2' in figure 4(b). Once released, these electrons can drift back to the conducting channel and restore the drain current, just as in the case of trap photoionization. Since the now-neutral acceptors are normally ionized in equilibrium, they rapidly capture an electron from a higher-lying deep level, as shown in figure 4(b). The net effect of this absorption—an electron returned to the 2DEG and a deep trap emptied—is the same as if the deep trap had been photoionized directly, as in transition '1'. It is clear, however, that while the ionized shallow acceptor provides a channel for the absorption and restoration of the drain current, it plays no role in trapping carriers and producing current collapse. Consequently, the 3.2 eV photoionization threshold cannot be viewed as the signature of a third deep trap responsible for the collapse. Similarly, light *above* the GaN bandgap also

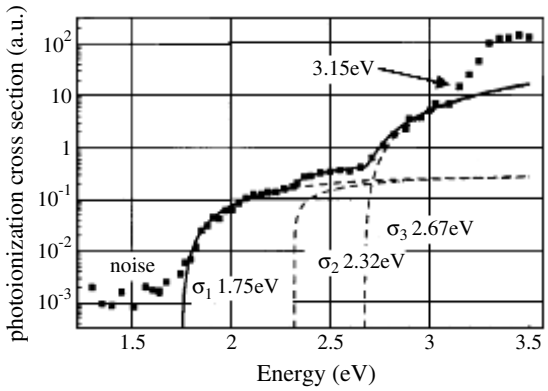

Figure 5. Photoionization spectrum of a GaN MESFET, exhibiting similar features as in figure 4(a), as well as an additional absorption threshold near 2.32 eV (after [30]).

restores the drain current by creating electron–hole pairs, transition '3' in figure 4(b): the photoexcited electron drifts back to the conducting channel as before while the hole is swept out of the charged region and is eventually captured by a filled deep level, as shown in the figure.

The spectral features in figure 4(a) are quite similar to the results of photocapacitance measurements of MOCVD-grown p^+–n and n-type GaN Schottky diodes reported by Hierro *et al* [28]. The three observed absorption features, with thresholds at 1.35, 2.64 and 3.22 eV below the conduction band, correspond well to the 1.8, 2.85 and 3.2 eV thresholds in figure 4(a). The differences in the 'threshold' energies determined occur because lattice relaxation was taken into account in analysing the photoionization results but was not considered for the photocapacitance data. The two deeper levels were not positively associated with a specific defect by Hierro *et al*, while the 3.22 eV threshold was identified as an unintentional shallow acceptor, such as Mg or C, in agreement with the discussion above.

Photoionization data on a MOCVD-grown GaN MESFET similar to that studied in figure 4(a) were reported by Meneghesso *et al* [29] and Armani *et al* [30] and are shown in figure 5. The data were interpreted as resulting from deep trapping centres in the GaN buffer layer or at the channel/buffer layer interface. Analysis of the spectrum rendered four ionization thresholds at 1.75, 2.32, 2.67 and 3.15 eV. The thresholds at 1.75 and 2.67 eV appear to compare well with Trap1 and Trap2, while the feature at 2.32 eV is not observed in the data of figure 4(a). The ionization threshold at 3.15 eV was associated with a deep, nonradiative defect on the basis of electroluminescence spectra from the same device, which exhibited no emission at that energy. This feature appears to be the same as the 3.2 eV absorption in figure 4(a), which we believe to be due to the photoneutralization of ionized shallow acceptors.

Superimposed on the spectrum in figure 4(a) are two sets of absorption data (full squares and diamonds) obtained from two independent measurements of persistent photoconductivity (PPC) in n-type GaN [31, 32]. That these spectra each follow the spectral dependence of Trap1 or Trap2 suggests that both of the deep centres involved in current collapse in GaN can participate in PPC as well—a characteristic shared by the DX centre in AlGaAs. Participation in PPC would also suggest that both traps have small cross-sections for carrier capture. The Trap2 absorption spectrum has also been shown [33] to agree very well with the photoluminescence excitation spectrum [34, 35] of yellow luminescence induced by carbon doping. This initial indication of an association of Trap2 with a carbon-related defect was investigated in more detail in [33] and is discussed in section 5.

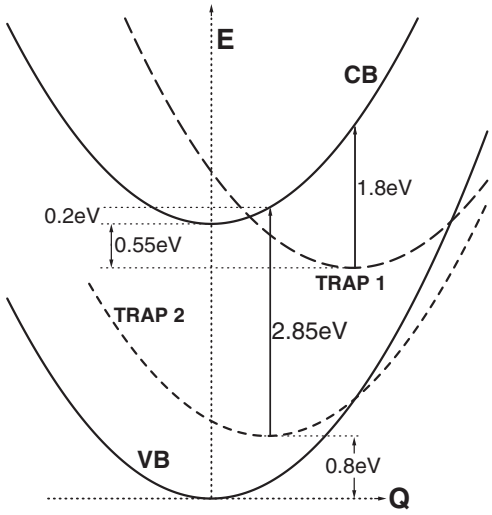

Figure 6. Approximate configuration coordinate diagram determined by fitting the spectral dependence in figure 4(a) for Trap1 and Trap2, using the analytical expression for the spectral dependence of the photoionization cross-section given in [26].

The photoionization threshold energies indicated in figure 4(a) suggest that Trap2 (2.85 eV) is very deep, while Trap1 (1.8 eV) lies somewhere near midgap [6]. However, the very large lattice relaxation associated with Trap1, manifested in the large Gaussian linewidth, leads to a different interpretation. From the Gaussian broadening, an estimate of the lattice relaxation energy of the two traps may be obtained. (This is more accurately determined by fitting the temperature dependence of the linewidth.) The Gaussian linewidth σ_G is given by [26]

$$\sigma_G = (2S\hbar\omega k_B T)^{1/2} \tag{3}$$

where $\hbar\omega$ is the phonon energy, S is the Huang–Rhys factor, k_B is the Boltzmann constant and T is the absolute temperature. The lattice relaxation (or Franck–Condon) energies $d_{FC} = S\hbar\omega$ determined from the fitted linewidths are found to be: $d_{FC} = 1.25$ and 0.2 eV for Trap1 and Trap2, respectively. The very large lattice relaxation energy of Trap1 is reminiscent of the DX centre in AlGaAs. From the ionization thresholds and lattice relaxation energies, a rough configuration coordinate diagram can be constructed, as shown in figure 6. It is apparent from the figure that, because of its large lattice relaxation energy, Trap1 is positioned well into the upper half of the bandgap. It would seem more appropriate, therefore, to view this defect as a strongly lattice-coupled deep donor rather than as a midgap state, which was inferred [6] from its 1.8 eV ionization threshold. While the configuration coordinate diagram for Trap1 is generally similar to the DX centre in AlGaAs [27] or the deep oxygen donor in AlGaN [18], there is currently no evidence to indicate that Trap1 is a DX-type defect. Because of its much smaller lattice relaxation energy ($\approx$0.2 eV), there is much less ambiguity in assigning Trap2 as a very deep acceptor state. The position of Trap2 in figure 6 is about 0.8 eV above the valence band. This is in good agreement with the carbon-related acceptor level reported by Ogino and Aoki [35] at $E_v + 0.87$ eV.

To gain further details about the traps responsible for current collapse in the GaN MESFET, saturation measurements were carried out for both Trap1 and Trap2. The results are shown in figure 7. For Trap1, with ionization threshold $\approx$1.8 eV (689 nm), the measurement of relative drain current increase with incident photon dose was carried out at 600 nm (2.07 eV), above the threshold for Trap1 but below that of Trap2. Thus only the portion of the drain current collapse

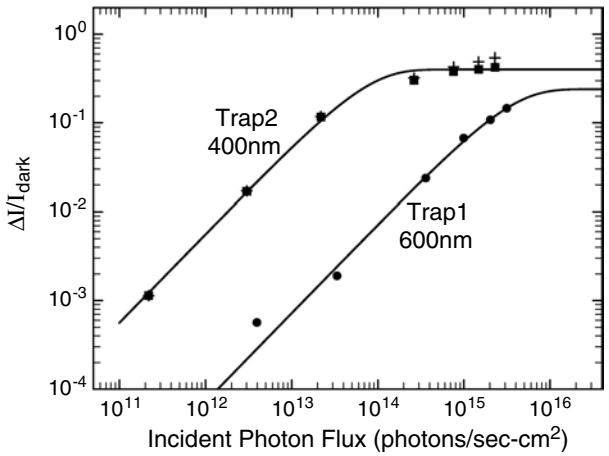

Figure 7. Photoionization saturation measurements in a GaN MESFET for a 5 s illumination time. The filled circles are experimental data taken at 600 nm (only Trap1 photoionized) and the + symbols are for 400 nm data (both traps photoionized). The squares indicate the Trap2 contribution to the latter. The full curves are fits to the data using equation (12).

associated with Trap1 could be restored. For Trap2, the use of 400 nm light (3.1 eV) led to the ionization of both traps. Under 400 nm illumination the drain current was observed to be restored to its value prior to collapse, as the carriers on both traps were released. Since 400 nm light fully restored the original drain current, any additional traps with threshold energies higher than 3.1 eV that could not be emptied by the 400 nm light would have to exist at very low concentrations. This confirms that the 3.2 eV absorption threshold is not associated with a defect that traps carriers during current collapse. As expected from the results of modelling that is detailed in the next section, the drain current increase observed in figure 7 exhibits a linear response at low incident light illumination and saturation at high illumination, when all of the traps have been ionized.

4.2. Analytical model

As noted earlier, the maximum drain current recovery ΔI that is measured in a saturation experiment at high illumination is directly related to the number of traps that are emptied, and hence to the total trap concentration. An analytical model of the recovery is necessary to extract such physically meaningful parameters and to understand the limits of the technique. The specific relationship between the optical response function $S(h\nu)$ and the trap photoionization cross-section may also be determined. The general approach, as employed in [7], is to derive the I–V characteristic of the MESFET in a manner parallel to typical textbook treatments [36, 37], but to add the charge distribution on the backside of the gate that results from the trapping of hot carriers. This distribution consists of the negatively charged region in the HR–GaN where hot carriers are trapped and the positive depletion region in the channel on the opposing side of the interface. The drain current increase ΔI results from the light-induced transfer of charge and the resulting reduction in the width of the backside channel depletion layer. In order to relate this to the incident photon dose, some consideration of the carrier dynamics during illumination will be required.

The distribution of trapped charge in the HR–GaN is expected to be centred near the drain end of the gate [23] where the electric field is the greatest. In order to simplify the analysis, a

uniform distribution of charge under the gate is considered. Conservation of charge transferred across the interface requires

$$Q_{\mathrm{T}} = eN_{\mathrm{d}}x_n = eN_{\mathrm{T}}x_{\mathrm{T}}, \tag{4}$$

where Q_{T} is the areal charge density initially transferred across the interface, e is the electronic charge, N_{d} and N_{T} are the (uniform) volume concentrations of donors in the channel and filled deep traps in the HR–GaN region, respectively, and x_n and x_{T} are the widths of the depletion and charged region layers, respectively. As the device is illuminated and electrons are released from the traps and return to the conducting channel, the density of trapped charge decreases. Thus, the trapped charge density becomes dependent upon the incident photon flux Φ and on the illumination time t: $Q = Q(\Phi, t)$. During illumination at constant Φ, the decreasing positive charge in the channel depletion region results in a decrease in the depletion layer width, as would occur, for example, during forward biasing. In the charged region, however, as trapped carriers are released by light, the remaining trapped charge cannot redistribute because the carriers are trapped at deep centres. Consequently, during illumination the response of the charged region is opposite to that of a conventional depletion region: the *depth* of the region remains fixed at x_{T} while the *concentration* decreases. Hence, as a function of illumination time, the areal concentration of trapped charge can be described as

$$Q(t) = eN_{\mathrm{d}}x_n(t) = eN^{-}(t)x_{\mathrm{T}}. \tag{5}$$

Here, $N^{-}(t)$ is the volume concentration of filled traps, while the concentration of the remaining uncharged (empty) traps is $N^{0}(t)$, such that $N^{-}(t) + N^{0}(t) = N_{\mathrm{T}}$.

For a drain voltage V applied to the device, the standard approach in determining the I–V relationship for the MESFET [36, 37] is to integrate the voltage drop along the length of the gate (y axis):

$$\mathrm{d}V = I_{\mathrm{D}}\,\mathrm{d}R = I_{\mathrm{D}}\frac{\mathrm{d}y}{N_{\mathrm{d}}e\mu_n W[d - x_n(y) - h(y)]}. \tag{6}$$

Here $x_n(y)$ and $h(y)$ are the widths of the depletion regions on the backside of the channel and under the gate, respectively, as a function of the position y along the length of the device. μ_n is the channel mobility, d is the thickness of the channel layer and W is the width of the device.

For $V_{\mathrm{GS}} = 0$ (the experimental condition), and for small drain voltages, i.e. *in the linear region of the I–V curve*, the width of the depletion and charged regions becomes independent of the drain voltage and position along the device. The widths of the depletion regions in the channel then become (see, e.g., [36, 37] and equation (5))

$$h = \sqrt{\frac{2\varepsilon}{eN_{\mathrm{d}}}V_{\mathrm{bi}}} \qquad x_n(t) = \frac{Q(t)}{eN_{\mathrm{d}}}, \tag{7}$$

where V_{bi} is the built-in potential associated with the gate contact and ε is the static dielectric constant. The time dependences of x_n and Q in equation (7) emphasize that these parameters will vary with light illumination. Using equation (7), integration of equation (6) gives the I–V relationship in the linear regime:

$$I_{\mathrm{D}}(t) = G_0 V\left[1 - \frac{h}{d} - \frac{Q(t)}{eN_{\mathrm{d}}d}\right] \tag{8}$$

where $G_0 = N_{\mathrm{d}}e\mu_n Wd/L$ is the channel conductance and L is the length of the gate. In order to construct the optical response function $S(h\nu)$ in equation (2), we require the drain current increase $\Delta I = I_{\mathrm{D}}(t) - I_{\mathrm{dark}}$ and the collapsed drain current I_{dark}:

$$\Delta I = \frac{G_0 V}{eN_{\mathrm{d}}d}[Q_{\mathrm{T}} - Q(t)] \qquad I_{\mathrm{dark}} = G_0 V\left[1 - \frac{h}{d} - \frac{Q_{\mathrm{T}}}{eN_{\mathrm{d}}d}\right]. \tag{9}$$

Thus, the optical response function takes the form

$$S(h\nu, t) = \frac{1}{\Phi t}\left[\frac{\Delta I}{I_{\text{dark}}}\right] = \frac{1}{\Phi t}\left[\frac{Q_{\text{T}} - Q_{h\nu}(t)}{eN_{\text{d}}d - \sqrt{2e\varepsilon N_{\text{d}} V_{\text{bi}}} - Q_{\text{T}}}\right], \tag{10}$$

and depends upon the initial amount of transferred charge, the illumination time and intensity and characteristics of the conducting channel. The explicit dependence of the trapped charge density on photon energy, indicated by $Q_{h\nu}(t)$, symbolizes the influence of the trap photoionization cross-section $\sigma(h\nu)$ on the efficiency of the light in restoring the drain current.

In order to apply equation (10) to the measured spectra, the time evolution of the trapped charge density, $Q_{h\nu}(t)$, must be determined. This is accomplished through a consideration of the carrier dynamics during illumination. The simple model employed, sketched in figure 8, assumes that all of the deep traps are initially filled. Photoionization of a given trap then leads to a conduction band electron that can either be recaptured by the empty traps left behind or drift back across the interface (under the influence of the built-in electric field formed by the nonequilibrium charge distribution) and restore the drain current. Careful consideration of deep level capture cross-sections in HR–GaN [7] suggests that, under the conditions of the photoionization measurements, the carrier capture rate is negligible compared to the rate of carrier drift. This follows from (1) the large electric field built up across the interface, $\approx 10^5$ V cm^{-1} [7] and (2) the relatively small capture cross-sections of these defects [7]. By neglecting carrier capture, $N^-(t)$ takes on a particularly simple form: $N^-(t) = N_{\text{T}} \exp[-\sigma(h\nu)\Phi t]$. The dependence of the trapped charge density on illumination time then becomes

$$Q(t) = eN^-(t)x_{\text{T}} = eN_{\text{T}}x_{\text{T}}\text{e}^{-\sigma(h\nu)\Phi t} = Q_{\text{T}}\text{e}^{-\sigma(h\nu)\Phi t}. \tag{11}$$

Equations (10) and (11) lead to an expression for the response function that can be compared directly to experiment:

$$S(h\nu, t) = \frac{1}{\Phi t}\left[\frac{\Delta I}{I_{\text{dark}}}\right] = \frac{1}{\Phi t}K[1 - \text{e}^{-\sigma(h\nu)\Phi t}], \tag{12}$$

where the parameter K depends only upon the initial trapped charge density and the characteristics of the channel:

$$K = \frac{Q_{\text{T}}}{eN_{\text{d}}d - \sqrt{2e\varepsilon N_{\text{d}} V_{\text{bi}}} - Q_{\text{T}}}. \tag{13}$$

Thus the total trap concentration $N_{\text{T}} = Q_{\text{T}}/ex_{\text{T}}$ is reflected in the optical response function $S(h\nu)$ through the parameter K, while the characteristic absorption spectrum of the trap enters through $\sigma(h\nu)$. Equation (12) may be employed directly to analyse saturation measurements of $\Delta I/I_{\text{dark}}$ versus incident photon dose Φt. The full curves in figure 7 were obtained in this way, with fitting parameters of σ_1 (600 nm) $= 6 \times 10^{-17}$ cm^2 and $N_1 = 4 \times 10^{11}$ cm^{-2} for Trap1 and σ_2 (400 nm) $= 2.8 \times 10^{-15}$ cm^2 and $N_2 = 6 \times 10^{11}$ cm^{-2} for Trap2. Thus, the two traps responsible for current collapse in the device in figures 4 and 7 occur in comparable concentrations but have very different photoionization cross-sections.

The spectral dependence of $S(h\nu)$ may be understood by considering equation (12) under conditions of weak carrier excitation (small photoionization cross section or low light level) such that $\sigma(h\nu)\Phi t \ll 1$. Under these conditions, equation (12) becomes

$$S(h\nu) \cong K\sigma(h\nu). \tag{14}$$

Thus, the optical response function $S(h\nu)$ is proportional to the photoionization spectrum of the deep trap (a condition necessary for meaningful spectroscopy) when the measurements are made under the following conditions: (1) the measurement of drain current increase is carried out within the linear portion of the I–V curve and (2) the measurement is made under weak

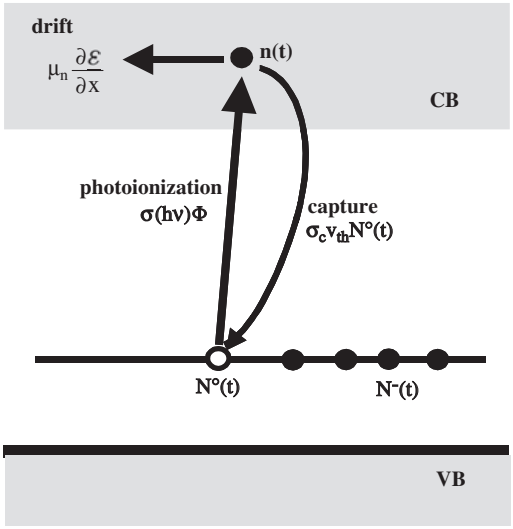

Figure 8. Carrier dynamics model employed in determining the dependence of the filled trap concentration on illumination time. Photoexcited carriers generated by the photoionization of filled traps are either recaptured at empty traps or drift back to the conducting channel to restore the drain current.

excitation, such that $\sigma(h\nu)\Phi t \ll 1$. The latter occurs when the incident photon dose is within the linear part of the saturation curve in figure 7. When measured under these conditions, the optical response function provides an absorption spectrum which is characteristic of the deep centre giving rise to the absorption.

When more than one defect is evident in the photoionization spectrum, as in figure 4(a), the optical response has been shown [7] to be a linear combination of contributions from the individual traps, e.g. $S(h\nu) = K_1\sigma_1(h\nu) + K_2\sigma_2(h\nu)$, where the K_j are identical to equation (13), except that Q_T in the numerator is replaced by Q_j, the areal density of charge trapped by defect j, and the $\sigma_j(h\nu)$ are the photoionization spectra of the individual traps.

4.3. Discussion

Through the analysis of photoionization data taken from GaN MESFETs, a detailed view of the nature of the defects responsible for current collapse in these devices becomes available. Two dominant traps appear to cause this phenomenon—Trap1 is most probably a strongly lattice-coupled deep donor, while Trap2 is a very deep acceptor that has been found (see section 5) to be a carbon-related defect. From spectral dependence and saturation measurements, it has been possible to determine the positions of these deep defects relative to the band edges, their concentrations, their photoionization cross-sections and an indication of their location within the device structure. In addition, the photoionization spectrum has been shown to provide a 'tag' that may be used to follow the response of the defect to varying external parameters or to associate the defect with other independent measurements that bear the identical absorption spectrum.

In contrast to the assignment of the absorption thresholds at 1.8 and 2.85 eV to strongly lattice-coupled deep defects, the absorption threshold at 3.2 eV was associated with the photoneutralization of ionized shallow acceptors. This conclusion was based on its threshold energy, which coincides with that of ionized acceptors in room temperature GaN, with the fact

that these absorptions are generally quite strong [38] for the unintentional shallow impurity concentrations ($\approx$mid $-$ 10^{16} cm^{-3}) found in HR–GaN, and with the fact that illumination *below* this energy threshold (400 nm, 3.1 eV) was shown to completely restore the collapsed drain current. The association of this threshold with a nonradiative deep centre [30], based on the lack of electroluminescence at this energy, is problematic in two respects:

(1) luminescence associated with the absorption of such a deep defect would be expected to be Stokes-shifted to lower energy by twice the lattice relaxation energy, $2d_{\mathrm{FC}}$, which can be hundreds of millielectronvolts, and
(2) a lack of observed luminescence can simply indicate that the transition is competing with a much stronger transition.

While the spectral dependence of the photoionization spectrum, e.g. figure 4(a), has been utilized to provide information about the defects involved, little mention has been made of the *magnitude* of the spectral features. Within the linear region of the I–V curve, equations (13) and (14) indicate that the magnitude of $S(h\nu)$ is proportional to the photoionization cross-section. The parameter K is essentially the ratio of the areal density of trapped charge to the sheet charge density in the channel under full collapse. The drain current in the linear regime is typically reduced anywhere from 5 to 50% during current collapse, resulting in a variation in K between 0.05 and 1 and a corresponding shift in $S(h\nu)$ by the same factor of 20. Thus, the value of K is generally less than, but roughly (within an order of magnitude) of the order of, unity. The order of magnitude of $S(h\nu)$ is then determined primarily by the photoionization cross-section. Variations in the trapped charge density Q_{T} (i.e. the amount of collapse) will change K, resulting in a shift of the level of the spectrum up or down within about an order of magnitude. As an example, figure 4(a) indicates that the magnitude of $S(h\nu)$ for Trap1 is much smaller than that of Trap2. Yet, it was concluded [7] that both traps are roughly equally responsible for the observed current collapse, as both defects occurred in comparable concentrations and were therefore able to trap comparable numbers of carriers. The large disparity in the optical response of the two traps reflects the large difference in their photoionization cross-sections (6×10^{-17} cm^2 versus 2.8×10^{-15} cm^2) rather than a large difference in their concentrations.

5. Photoionization spectroscopy in GaN HEMTs

5.1. Photoionization measurements

It is apparent from the AlGaAs/GaAs literature [14–16] and from earlier work on AlGaN/GaN devices [19, 21] that HEMTs are also affected by current collapse. The responsible defects could reside on the surface, in the AlGaN layer, at the hetero-interface or in the HR–GaN barrier. Photoionization spectroscopy has been useful in determining the location and characteristics of the responsible traps. Initial measurements were carried out in several MOCVD-grown HEMTs exhibiting a significant amount of collapse. These studies concluded [39] that the same HR–GaN layer traps that were found responsible for collapse in the MESFET were also the cause of current collapse in the HEMT. A typical photoionization result for the HEMT is shown in figure 9 (full circles) and is compared (open circles) to the photoionization spectrum of the GaN MESFET shown in figure 4(a). The same broad spectral features (Trap1, Trap2) and the 3.2 eV shallow acceptor threshold are observed, just as in the GaN MESFET. The rapid increase at the GaN bandgap and the lack of response at the AlGaN bandgap confirm that the traps reside in the HR–GaN layer.

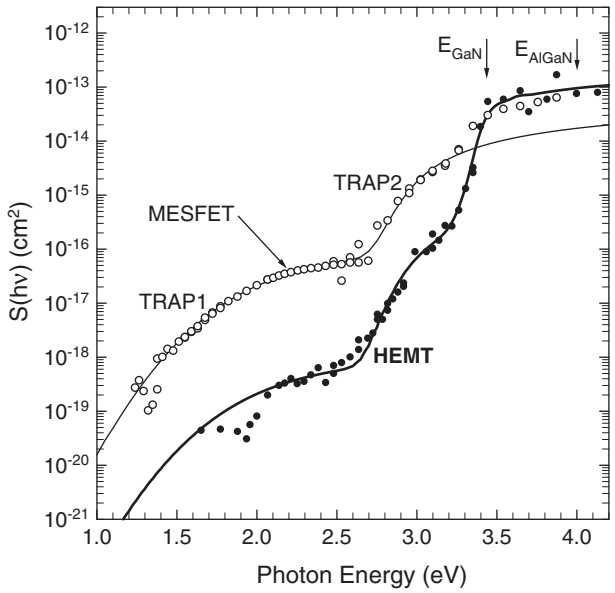

Figure 9. Photoionization spectrum of an AlGaN/GaN HEMT structure (filled circles) compared to that of the GaN MESFET (open circles) in figure 4(a). The HEMT device exhibits the same two broad features, Trap1 and Trap2, that were observed in the MESFET.

The origin of these HR–GaN layer traps is of particular interest. A possible association of Trap2 with carbon was noted earlier, based on the coincidence of the Trap2 photoionization spectrum and a carbon-related absorption appearing in yellow luminescence excitation spectroscopy [34, 35]. In order to investigate this possibility in more detail, several HEMT wafers were fabricated [33] by MOCVD with their HR–GaN layers grown at varying pressures. The growth pressure affects the incorporation of deep defects. In particular, it is known that lower pressure growth leads to higher defect concentrations and HR material. Lower pressure also enhances the incorporation of carbon [40, 41] into the MOCVD layers. In fact, recent studies have concluded independently that carbon doping introduces a deep centre into GaN that is responsible for the high resistivity material [42].

The dc I–V characteristics of the HEMT structures grown on these wafers exhibited varying degrees of current collapse. Photoionization spectra for devices grown at three HR–GaN growth pressures are shown in figure 10(a). The data exhibit an increasingly stronger Trap2 contribution as the pressure is lowered, while the Trap1 feature is only weakly affected [33]. This is consistent with the association of Trap2 with carbon, which incorporates more readily at lower pressures. A more detailed investigation was made by studying the growth pressure dependence of the deep trap concentrations using photoionization saturation measurements. The results of these measurements are shown in figure 10(b) for four growth pressures. Two illumination wavelengths, 633 and 400 nm, were employed to separate the contributions from the two traps. The full lines are fits to the data using an analysis similar to that described in section 4.2 for the MESFET, although some changes in approach were necessary to apply this modelling technique to the HEMT. A detailed description of this modelling approach is presented in section 5.2. The dependences of the areal concentrations of Trap1 and Trap2 on growth pressure, determined using this model, are shown in figure 11 and are compared to the volume concentration of carbon in the HR–GaN layers, as measured

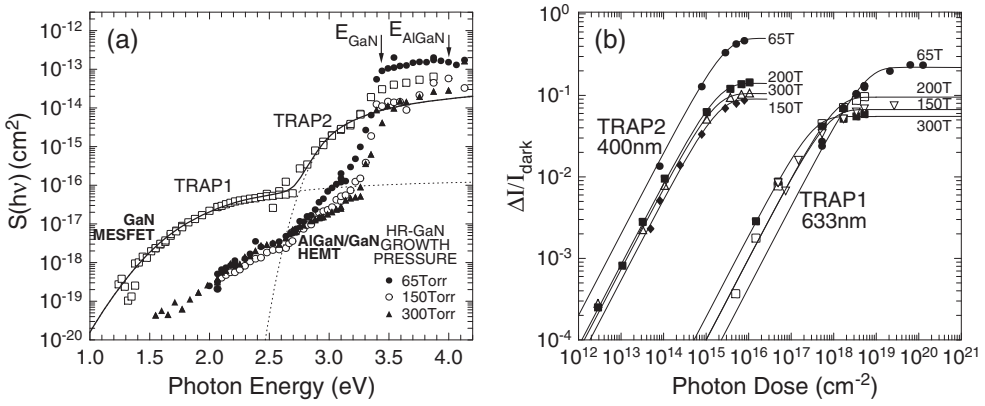

Figure 10. (a) Photoionization spectra of MOCVD-grown AlGaN/GaN HEMT structures with HR–GaN layers grown at different pressures. The spectrum of a GaN MESFET is shown for comparison. (b) Photoionization saturation measurements taken with 633 and 400 nm light for HEMTs with HR–GaN layers grown at four different pressures. The full curves are fits of the data using equations (21) and (22).

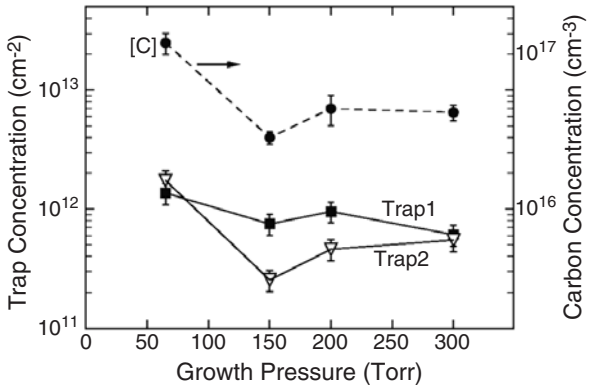

Figure 11. Dependence on the HR–GaN layer growth pressure of the areal concentrations of Trap1 (filled squares) and Trap2 (open triangles), determined from fitting the data in figure 10(b) using equations (21) and (22). The growth pressure dependence of the volume concentration of carbon in the HR–GaN layer, as determined by SIMS measurements on the same materials, is shown for comparison.

by secondary ion mass spectrometry (SIMS). It is apparent from the figure that the Trap2 concentration tracks that of carbon, and a plot of the Trap2 concentration versus that of carbon exhibits a linear dependence [33]. This represents strong evidence for the association of Trap2 with a carbon-related defect. The dependence of the Trap1 concentration on growth pressure is considerably weaker than that of Trap2 and not well-correlated with the concentration of carbon or with any of the other common impurities for which SIMS measurements were carried out. At the present time Trap1 has not been associated with a specific defect.

It is interesting that the 2DEG sheet charge, n_s, for this set of devices exhibited [43] the same dependence (but inverted) on growth pressure as the total trap concentration (i.e. Trap1 + Trap2). The inverse correlation between sheet charge and total trap concentration suggests that, during the formation of the 2DEG, the presence of deep traps reduces the sheet charge to the value that is measured in the completed devices. This observation indicates

that the traps that degrade device performance by limiting the maximum attainable n_s are the *same* traps that cause current collapse. It is reasonable to assume that the traps responsible for reducing the 2DEG sheet charge during growth are the dominant compensating deep centres in the HR–GaN. Since these are the same traps that cause current collapse, it follows that Trap1 and Trap2 must be the deep centres primarily responsible for compensation in the HR–GaN.

The involvement of a carbon-related defect (i.e. Trap2) in the compensation mechanism of n-type and HR–GaN has been an issue for some time. Ogino and Aoki [35] concluded, after very detailed optical studies published almost 25 years ago, that the introduction of carbon in GaN produces a deep acceptor level at about 0.87 eV above the valence band maximum—in very good agreement with the position of Trap2. This was attributed to a V_{Ga}–C_N defect centre. Calculations by Neugebauer and Van de Walle [44] suggested that, while this complex could form a deep acceptor level in GaN, it would be unstable due to a very high formation energy, except under extreme n-type conditions. Still, carbon doping was shown by Tang *et al* [45] to be effective in producing HR material in MBE-grown GaN. These layers were subsequently used as substrates to fabricate high-quality HEMT devices [46]. While it is clear that the introduction of carbon can lead to HR–GaN, the association with a specific compensating deep defect has been elusive. Recent detailed calculations by Wright [47] confirmed the view that V_{Ga}–C_N should be unstable. No alternative deep acceptor state was proposed, as the main compensation mechanism in n-type and HR–GaN was viewed [47, 48] as resulting from self-compensation between C_{Ga} and C_N when the carbon content exceeded that of the dominant shallow donor (e.g. Si). A photoluminescence emission observed centred at 3 eV was associated [48] with C_{Ga}–C_N transitions. These conclusions are clearly at odds with the view that compensation in HR–GaN results from a deep acceptor, such as Trap2 or the centre proposed by Ogino and Aoki. While it is possible that both mechanisms contribute simultaneously, a definitive determination of the dominant compensation mechanisms in HR–GaN is still needed to clarify our present understanding.

Photoionization spectroscopy studies have recently been carried out by Wolter *et al* [49–51] on several MOCVD-grown AlGaN/GaN HEMT devices, most of which employed doped AlGaN barrier layers. Spectra obtained in these studies exhibit features similar to those in figures 9 and 10(a) for photon energies $h\nu > 2.5$ eV, as shown in figure 12. For lower energies, no drain current increase is observable. The authors have interpreted this in terms of photoconductivity quenching by a hole trap in the GaN buffer layer. This occurs when the incident light, in addition to ionizing the trapped carriers to the conduction band, promotes valence band electrons to the hole trap levels. This leads to recombination of the resulting valence band holes with the conduction band electrons. During the photoionization spectroscopy measurement, photoexcited electrons released from the deep traps recombine with the valence band holes before they can return to the 2DEG. This leads to a quenching of the light-induced drain current increase. Such a hole trap, in a broad spectral range around 1–2 eV, has been reported [52] recently in n-GaN. It is interesting that, while some of the photoionization spectra in figure 10(a) do appear to reflect this effect, others do not. The hole trap associated with this photoconductivity quenching is apparently quite sensitive to the growth conditions of the HR–GaN layer.

In the region $h\nu > 2.5$ eV, Wolter *et al* [50, 51] observed photoionization spectra with thresholds quite similar to those described above at 2.85 and 3.2 eV. Both of these transitions were interpreted as photoionization from deep trap levels. We have argued, however, that the 3.2 eV transition is associated with the photoneutralization of residual ionized shallow acceptors in the GaN layer, as explained in section 4.1. Hierro *et al* [28] have also taken this view. The spectral position of this feature is indicative of a shallow level. In addition, illumination with 400 nm light (3.1 eV), which is below the 3.2 eV absorption threshold,

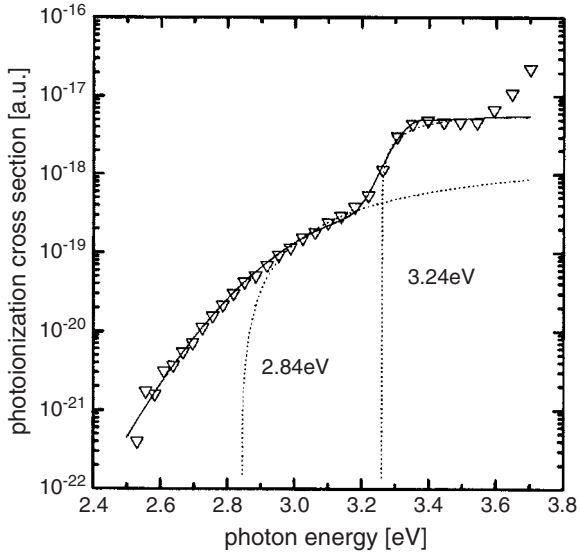

Figure 12. Photoionization spectrum (triangles) of a doped AlGaN/GaN HEMT structure. The data are fitted either with (full curves) or without (dotted curves) Gaussian broadening included (after [50]).

has been shown to completely restore the collapsed drain current [33]. Thus, no substantial concentration of traps with ionization threshold energies higher than 3.1 eV can contribute significantly to the observed current collapse. The effect of the optical transitions just above the 3.2 eV threshold is to excite an electron from the ionized acceptor to the conduction band, resulting in a free electron and a neutral shallow acceptor. As we noted earlier, the electron drifts back to the channel and increases the 2DEG sheet charge, while the nonequilibrium neutral acceptor captures an electron from a higher-lying deep level (see, e.g., figure 4(b)). The net effect (empty deep level and increased 2DEG sheet charge) is the same as if the photoionization took place at the deep level. However, it is clear that the shallow acceptor level at 3.2 eV plays no role in trapping carriers and causing current collapse, as it is a shallow acceptor level and already filled in equilibrium.

Wolter *et al* [51] have also reported an interesting investigation of the effect on the photoionization spectra of gate bias and of the spatial separation between the 2DEG and the surface [50]. They observe that:

(i) for devices where the 2DEG is closer to the AlGaN surface, the drain current is lower and the response function $S(h\nu)$ in the photoionization spectrum is raised, suggesting a higher trap concentration, and
(ii) as the gate bias is reduced (i.e. made more negative), $S(h\nu)$ increases, as shown in figure 13, again indicating the involvement of a larger number of traps.

These observations have been interpreted [50, 51] as evidence that the traps responsible for the collapse are on the surface of the AlGaN. The correspondence between the spectral features of the photoionization spectra in figures 9 and 12 confirms that the deep trap involved in these measurements is identical to that of Trap2 discussed earlier. There is, therefore, a differing view of the location and nature of the defect associated with the 2.85 eV threshold. As discussed above, the 2.85 eV absorption threshold (Trap2) has been associated with the HR–GaN layer in several ways:

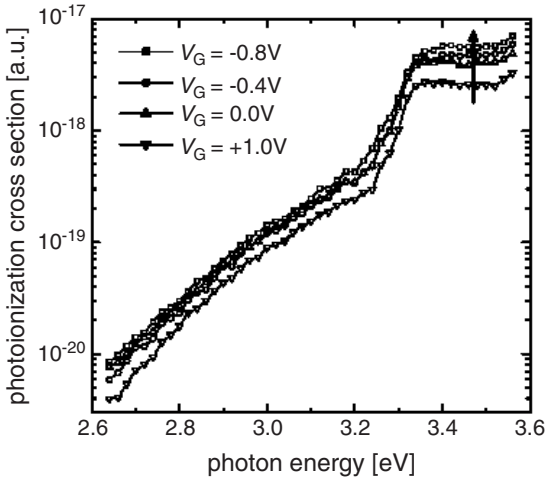

Figure 13. Photoionization spectrum of a doped AlGaN/GaN HEMT structure as a function of applied gate bias (after [51]).

(i) it has been well-correlated with the concentration of carbon in the HR–GaN buffer layer of AlGaN/GaN HEMTs [33],

(ii) the Trap2 spectrum has been observed in PPC studies of n-GaN [32] and in luminescence excitation spectroscopy of GaN:C [34, 35], and

(iii) Trap2 has been observed in the photoionization spectra of GaN MESFETs [6].

These results are inconsistent with an AlGaN surface trap. In the latter two cases, the trap cannot be located on an AlGaN surface, since no AlGaN surface exists, while the former case is specifically associated with the HR–GaN layer.

5.2. Analytical model

In order to analyse the results of photoionization saturation measurements in HEMT structures, an analytical model of the light-induced drain current recovery is required, similar to that developed in section 4.2 for the MESFET. In the case of the MESFET, the effect of hot channel carrier injection and trapping in the neighbouring HR–GaN layer was to create a positive depletion region in the conducting channel that increased the resistance of the channel, thus reducing the drain current. Since the conducting channel in a HEMT device is a 2DEG, this approach must be altered slightly in order to model the effect of hot carrier injection on the device output characteristics. The approach taken here follows that of [8].

In the HEMT, the effect of current collapse is to transfer from the channel (through hot carrier injection) a fraction of the sheet charge in the high-field region of the 2DEG between the gate and drain, where hot carrier effects are maximum. The resistance associated with this portion of the channel increases accordingly and can dominate the total channel resistance when the device is fully collapsed. Then, for subsequent measurements (within the linear region of the I–V curve), the drain current becomes proportional to the sheet charge, n_s, in this region [53]. While this approximation begins to break down once the incident light has restored most of the collapsed drain current, this simple approach still provides a useful method for analysing light illumination measurements in HEMT structures. The concentration

of trapped charge is also assumed for simplicity to be uniform along the length of the structure, thereby neglecting the charge localization near the drain end of the gate.

With these simplifications, the drain current prior to collapse, I_d, and the fully collapsed drain current before light illumination, I_{dark}, are written for the linear part of the I–V curve in the form

$$\begin{aligned} I_d &= AV_{ds}n_s \\ I_{dark} &= AV_{ds}(1-\beta)n_s, \end{aligned} \tag{15}$$

where β is the fraction of the original sheet charge n_s that is trapped by deep defects, V_{ds} is the applied drain bias and all other parameters have been lumped into A. The total areal concentration of filled deep traps is then

$$n_T = \beta n_s = n^-(t) + n^0(t), \tag{16}$$

where n^- and n^0 are the (illumination-time-dependent) areal concentrations of filled and empty deep traps, respectively. If all of the traps are considered initially filled (i.e. the device is fully collapsed), then $n^-(0) = n_T$.

When the collapsed device is illuminated with light above the photoionization threshold of the trap, some of the trapped carriers are released and return to the 2DEG to partially restore the drain current. The increase in sheet charge, Δn_s, is equal to the light-induced loss in the areal density of trapped charge:

$$\Delta n_s(\Phi, t) = n_T - n^-(\Phi, t), \tag{17}$$

where we have made explicit the dependence on the incident photon flux Φ and the illumination time t. The fractional increase in the drain current above the collapsed level due to light illumination of photon energy $h\nu$, $\Delta I/I_{dark} = [I_d(h\nu) - I_{dark}]/I_{dark}$, can then be constructed from equations (15) and (17):

$$\frac{\Delta I(h\nu)}{I_{dark}} = \frac{n_T - n^-(\Phi, t)}{(1-\beta)n_s}. \tag{18}$$

As in the modelling for the GaN MESFET in section 4.2, the expression of the fractional drain current increase due to light illumination requires consideration of the carrier dynamics during the illumination in order to obtain an expression for the time dependence of the filled trap concentration, $n^-(t)$. We employ the same carrier dynamics model as in the case of the MESFET, where the photoexcited carrier recapture rate is much less than the rate of return of the carriers to the conducting channel (see, e.g., figure 8). This results in an exponential decay of the filled trap concentration analogous to equation (11):

$$n^-(t) = n_T e^{-\sigma(h\nu)\Phi t} \tag{19}$$

where $\sigma(h\nu)$ is the photoionization cross-section of the trap. From equations (18) and (19), the fractional drain current increase reflects the same exponential growth as in the case of the MESFET:

$$\begin{aligned} \frac{\Delta I}{I_{dark}} &= B(1 - e^{-\sigma(h\nu)\Phi t}) \\ B &= \frac{\beta}{1-\beta}. \end{aligned} \tag{20}$$

Equation (20) may be employed to analyse photoionization measurements of the fractional drain current increase, $\Delta I/I_{dark}$, versus photon dose Φt. The fitting parameters are B and σ. B is related to the total trap concentration through $n_T = \beta n_s$ and the sheet charge of the device can be determined independently by Hall effect measurements.

This analysis assumes that a single trap is responsible for the collapse. A simple extension to N traps, where the incident photon energy is greater than the ionization threshold of the first $j = 1$ through k traps ($k \leqslant N$), leads to [8]

$$\frac{\Delta I}{I_{\text{dark}}} = \sum_{j=1}^{k} B_j (1 - \mathrm{e}^{-\sigma_j(h\nu)\Phi t}) \tag{21}$$

and

$$B_j = \frac{\beta_j}{1 - \beta}. \tag{22}$$

The index $j = 1$–N labels the individual traps, $\sigma_j(h\nu)$ is the photoionization cross-section for trap j at photon energy $h\nu$, β_j is the fraction of the 2DEG sheet charge trapped on trap j and $\beta = n_{\text{T}}/n_{\text{s}} = \Sigma_j \beta_j$. Equations (21) and (22), which can be applied directly to photoionization saturation data involving two or more traps, are analogous to equations (12) and (13) for the MESFET.

Analysis of the data in figure 10(b) using equations (21) and (22) led to the determination of the growth pressure dependence of the Trap1 and Trap2 concentrations shown in figure 11. The extracted photoionization cross-sections for Trap1 and Trap2, $\approx 10^{-18}$ and 6×10^{-16} cm^2, respectively, differ by a factor of about 600, which is the origin of the large shift between the 400 and 633 nm data along the horizontal axis in figure 10(b).

6. Photoionization spectroscopy of current collapse induced by bias stress

As we have noted earlier, current collapse degrades the performance of nitride-based MESFETs and HEMTs. In our laboratory, we have observed that devices grown by MOCVD generally show some measurable amount of collapse (which can vary from nominal to substantial), while MBE-grown devices usually exhibit little or no collapse. This may be in part a result of the organic precursors employed in MOCVD growth that introduce substantial concentrations of carbon into the material, particularly at low growth pressures [40, 41]. However, it has recently been reported [54] that current collapse can also be *induced* in devices that initially show little or no collapse by exposing the device to stress, i.e. by applying a high dc drain–source bias for an extended period of time (several hours). This phenomenon represents a potential reliability issue for these devices.

The I–V characteristics of a MBE-grown HEMT (shown in figure 14) demonstrate this effect [54]. Two sets of three consecutive I–V sweeps are shown: the set of broken curves was taken before stress and the set of full curves was taken after stress. Toward the end of the first I–V sweep of each set, the device is exposed to a high drain–source voltage, which can lead to hot carrier injection and trapping. This collapsed state is probed in the two subsequent sweeps. Before stress (broken curves), there is only a small decrease in drain current in the subsequent two sweeps, indicating little current collapse. After stress (full curves) there is a large decrease in drain current that reflects substantial current collapse induced by the prolonged bias stress. In devices that already exhibit some current collapse before stress, the effect of the stress is to increase the severity of the collapse.

Since current collapse occurs when empty deep traps exist at equilibrium, and are therefore capable of trapping injected hot carriers, the effect of this applied stress must be to create such traps. This can occur either (a) directly, through the creation of deep defects by hot carrier damage [55, 56], or (b) existing deep traps, which are filled and thus 'inactive', can be activated as a result of the stress. The latter effect can occur by a hot-carrier-induced lowering of the Fermi level. Here, hot carrier damage creates defects that are lower in the bandgap than the

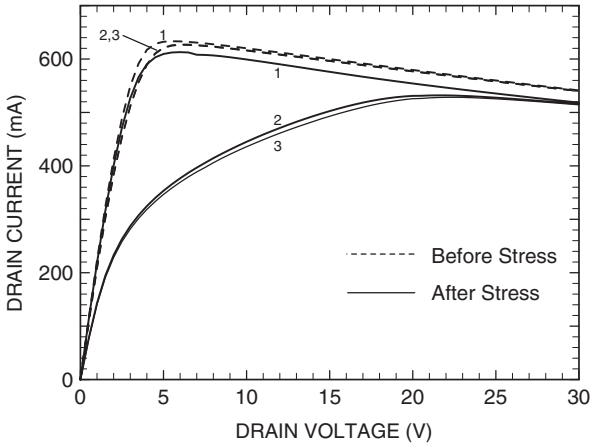

Figure 14. Sequence of three I–V sweeps for a MBE-grown AlGaN/GaN HEMT structure, both before (broken curves) and after (full curves) 16 h of drain bias stress.

deep centres. The deep traps then empty into the newly created lower-lying defects and are thus available to trap injected carriers.

In order to investigate the nature of the traps that are induced during stress, photoionization measurements were carried out on both MBE- and MOCVD-grown HEMTs. Devices that exhibited little or no collapse before stress were chosen for study, so that the measured drain current recovery was only representative of the traps associated with the collapse induced by the stress. The resulting photoionization spectra are shown in figure 15. In the figure, spectra from a MOCVD GaN MESFET (open squares) and a typical, unstressed MOCVD HEMT (open circles) are shown for comparison. The spectrum of the stressed MOCVD device (full circles) is very similar to that of the unstressed MOCVD device, i.e. they exhibit the same spectral features. This would suggest that the same traps are responsible for the collapse in both cases. The spectrum of the MBE-grown HEMT (full squares) is very different: there is no Trap2 feature evident and a new absorption threshold is observed near 3.7 eV, above the GaN bandgap.

Since for MOCVD-grown structures the same traps are involved for both unstressed and stressed devices, it seems unlikely that the effect of the stress is to create precisely the same traps that were already observed in unstressed devices. It is more likely that these traps already existed, but were filled before the stress, as in (b) above.

For MBE-grown devices, the absence of a Trap2 feature in the photoionization spectrum is consistent with the association of this absorption with a carbon-related defect [33], as a substantial concentration of inadvertent carbon impurities is not expected in MBE-grown material. The absorption threshold at 3.7 eV is above the GaN bandgap and must therefore be associated with the AlGaN layer. Since the conducting channel is a 2DEG, this absorption must lead to photoexcited electrons in the conduction band of the AlGaN ($x = 0.25$, $E_g \approx 3.9$ eV). This places the electronic state of the defect roughly 0.2 eV above the AlGaN valence band. This is too shallow to be a deep defect, but is in the same energy range as shallow acceptors in AlGaN. Consequently, the 3.7 eV threshold does not appear to be associated with a deep centre that could result in current collapse, but instead corresponds to the photoneutralization of ionized shallow acceptors, similar to the 3.2 eV photoionization threshold in GaN. Since the Trap1 defect and the 3.7 eV threshold were the only features in the photoionization spectrum that could be associated with the collapse, the sole trapping centre that is responsible for stress-induced current collapse in MBE-grown HEMTs must be Trap1, a GaN buffer layer defect [6, 7].

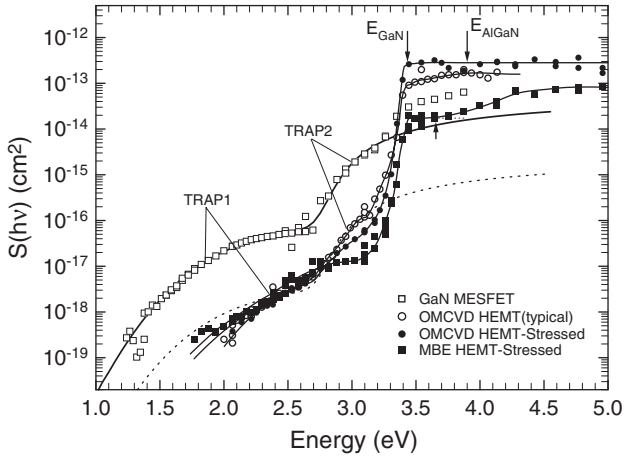

Figure 15. Photoionization spectra of current collapse induced by dc bias stress in HEMTs exhibiting little collapse before stress, and grown by both MOCVD (full circles) and MBE (full squares). These spectra are compared to those of MOCVD-grown MESFET and HEMT devices (open squares and circles, respectively) that exhibited current collapse but were not stressed.

7. Summary

This review has focused on the detailed characterization and identification of the deep defects that are responsible for current collapse in state-of-the-art nitride-based FETs. The origins of current collapse have been discussed and compared to similar phenomena observed in devices fabricated from AlGaAs/GaAs and other earlier material systems. The concept of photoionization spectroscopy is introduced and developed with the emphasis on the connection between the measured drain current increase and the intrinsic optical properties of the deep traps causing the collapse. Recent experimental results in GaN MESFETs and AlGaN/GaN HEMTs are described and the implications regarding the nature of the defects responsible are discussed. Models of light-induced drain current restoration appropriate to the MESFET and HEMT are developed to provide a basis for the technique and to enable the extraction of physically significant trap characteristics from the data. Finally, recent investigations of current collapse induced by short-term (several hours) bias stress in AlGaN/GaN HEMTs are described and analysed with reference to similar measurements in the unstressed devices.

From these studies, it has been determined that, in the case of the MOCVD-grown GaN MESFET, two deep traps are responsible for the collapse. These have been labelled as Trap1 and Trap2, with photoionization thresholds at 1.8 and 2.85 eV, respectively. These traps were both found to reside in the HR–GaN buffer layer and are deep and strongly lattice-coupled. Analysis of these absorption spectra suggests that Trap1 is a strongly lattice-coupled deep donor. A third absorption threshold at 3.2 eV, just below the GaN bandgap, was associated with the photoneutralization of ionized shallow acceptors and was not representative of a third deep trap that could lead to current collapse.

Photoionization spectra from MOCVD-grown AlGaN/GaN HEMTs exhibit spectral features very similar to that of the MESFET, indicating that the same two GaN buffer layer traps are responsible for current collapse in the HEMT structure. The dependence of the Trap2 concentration on the carbon content of the HR–GaN layer indicates that Trap2 is a carbon-related defect in the GaN buffer layer of the HEMT structure.

Photoionization spectra of current collapse induced by short-term bias stress were obtained from HEMTs grown by both MOCVD and MBE. The spectra of the MOCVD devices exhibited

the same spectral features seen in unstressed devices, indicating that the same traps were responsible for the collapse. It was concluded that these traps were most probably present (but occupied) in the devices before stress, and emptied as a result of the stress. In MBE-grown devices, Trap2 is not observed, due to the lack of a significant source of unintentional carbon impurities in the MBE growth system. A new absorption at 3.7 eV was associated with the AlGaN barrier. This feature was identified as a photoneutralization of AlGaN shallow acceptors, analogous to the 3.2 eV absorption in GaN, and not associated with a deep defect that could result in current collapse. Consequently, the only feature in the photoionization spectrum of MBE-grown devices that is interpreted to be related to a deep centre is that of Trap1. Thus, Trap1 appears to be solely responsible for current collapse induced by stress in MBE-grown devices.

Acknowledgments

Much of the work described above would not have been possible without important contributions from a number of people. The authors are indebted to D Koleske, A Wickenden and R Henry for their efforts in MOCVD growth and to D S Katzer and D Storm for the growth of the MBE device structures. We would also like to thank K Ikossi and J Roussos for their help in device fabrication and characterization and J Mittereder for much hard work in preparing and characterizing the bias-stressed devices. Finally, we would like to thank J Freitas Jr for his contributions during the initial stages of this work and H Dietrich, J Albrecht, P Ruden and W Kruppa for several fruitful discussions on various aspects of these studies. This work was supported by the Office of Naval Research.

References

[1] Zolper J C 1999 *Int. Electron Device Mtg Digest* (Piscataway, NJ: IEEE) pp 389–92
[2] Wu Y-F, Kapolnek D, Ibbetson J, Zhang N-Q, Parikh P, Keller B P and Mishra U K 1999 *Int. Electron Device Mtg Digest* (Piscataway, NJ: IEEE) pp 925–7
[3] Binari S C, Klein P B and Kazior T E 2002 *Proc. IEEE* **90** 1048–58
[4] Kohn E, Daumiller I, Schmid P, Nguyen N X and Nguyen C N 1999 *Electron. Lett.* **35** 1022–3
[5] Vetury R, Zhang N Q, Keller S and Mishra U K 2001 *IEEE Trans. Electron Devices* **48** 560–6
[6] Klein P B, Freitas J A Jr, Binari S C and Wickenden A E 1999 *Appl. Phys. Lett.* **75** 4016–8
[7] Klein P B, Binari S C, Freitas J A Jr and Wickenden A E 2000 *J. Appl. Phys.* **88** 2843–52
[8] Klein P B 2002 *J. Appl. Phys.* **92** 5498–502
[9] Ning T H, Osburn C M and Yu H N 1977 *J. Electron. Mater.* **6** 65–76
[10] Forbes L, Sun E, Alders R and Moll J 1979 *IEEE Trans. Electron Devices* **26** 1816–8
[11] Luo F C 1979 *J. Vac. Sci. Technol.* **16** 1045–8
[12] Wysocki J J 1982 *IEEE Trans. Electron Devices* **29** 1798–805
[13] Fischer R, Masselink W T, Henderson T, Klem J, Arnold D and Morkoc H 1984 *IEEE Trans. Electron Devices* **31** 1963–4
[14] Drummond T J, Fischer R J, Kopp W F, Morkoc H, Lee K and Shur M S 1983 *IEEE Trans. Electron Devices* **30** 1806–11
[15] Fischer R, Drummond T J, Klem J, Kopp W, Henderson T S, Perrachione D and Morkoc H 1984 *IEEE Trans. Electron Devices* **31** 1028–31
[16] Kastalsky A and Kiehl R A 1986 *IEEE Trans. Electron Devices* **33** 414–23
[17] Ridley B K 2000 *Appl. Phys. Lett.* **77** 990–92
[18] McCluskey M D, Johnson N M, Van de Walle C G, Bour D P, Kneissl M and Walukiewicz W 1998 *Phys. Rev. Lett.* **80** 4008–11
[19] Khan M A, Shur M S, Chen Q C and Kuznia J N 1994 *Electron. Lett.* **30** 2175–6
[20] Binari S C, Kruppa W, Dietrich H B, Kelner G, Wickenden A E and Freitas J A Jr 1997 *Solid-State Electron.* **41** 1549–54

[21] Binari S C, Ikossi-Anastasiou K, Roussos J A, Park D, Koleske D D, Wickenden A E and Henry R L 2000 *Proc. Int. Conf. GaAs Manufacturing Tech.* (Piscataway, NJ: IEEE) pp 201–4
[22] Binari S C, Ikossi K, Roussos J A, Kruppa W, Park D, Dietrich H B, Koleske D D, Wickenden A E and Henry R L 2001 *IEEE Trans. Electron Devices* **48** 465–71
[23] Zhang L, Lester L F, Baca A G, Shul R J, Chang P C, Willison C G, Mishra U K, Denbaars S P and Zolper J C 2000 *IEEE Trans. Electron Devices* **47** 507–11
[24] Inkson J C 1981 *J. Phys. C: Solid State Phys.* **14** 1093–101
[25] Lucovsky G 1965 *Solid State Commun.* **3** 299–302
[26] Jaros M 1977 *Phys. Rev.* B **16** 3694–706
[27] Mooney P M, Northrup G A, Morgan T N and Grimmeiss H G 1988 *Phys. Rev.* B **37** 8298–307
[28] Hierro A, Kwon D, Ringel S A, Jansen M, Speck J S, Mishra U K and DenBaars S P 2000 *Appl. Phys. Lett.* **76** 3064–6
[29] Meneghesso G, Chini A, Zanoni E, Manfredi M, Pavesi M, Boudart B and Gaquiere C 2000 *Proc. Int. Electron Devices Mtg* (Piscataway, NJ: IEEE) pp 16.5.1–4
[30] Armani N, Grillo V, Salviati G, Manfredi M, Pavesi M, Chini A, Meneghesso G and Zanoni E 2002 *J. Appl. Phys.* **92** 2401–5
[31] Reddy C V, Balakrishnan K, Okumura H and Yoshida S 1998 *Appl. Phys. Lett.* **73** 244–6
[32] Hirsch M T, Wolk J A, Walukiewicz W and Haller E E 1997 *Appl. Phys. Lett.* **71** 1098–100
[33] Klein P B, Binari S C, Ikossi K, Wickenden A E, Koleske D D and Henry R L 2001 *Appl. Phys. Lett.* **79** 3527–9
[34] Reuter E E, Zhang R, Kuech T F and Bishop S G 1999 *MRS Internet J. Nitride Semicond. Res.* **4S1** G3.67
[35] Ogino T and Aoki M 1980 *Japan. J. Appl. Phys.* **19** 2395–405
[36] Sze S M 1981 *Physics of Semiconductor Devices* (New York: Wiley) p 77
[37] Grove A S 1967 *Physics and Technology of Semiconductor Devices* (New York: Wiley) p 159
[38] Ridley B K 1993 *Quantum Processes in Semiconductors* (Oxford: Clarendon) p 199
[39] Klein P B, Binari S C, Ikossi-Anastasiou K, Koleske D D, Wickenden A E, Henry R L and Katzer D S 2001 *Electron. Lett.* **37** 661–2
[40] Koleske D D, Wickenden A E, Henry R L and Twigg M E 2002 *J. Cryst. Growth* **242** 55–69
[41] Parish G, Keller S, DenBaars S P and Mishra U K 2000 *J. Electron. Mater.* **29** 15–20
[42] Webb J B, Tang H, Rolfe S and Bardwell J A 1999 *Appl. Phys. Lett.* **75** 953–5
[43] Klein P B, Binari S C, Ikossi K, Wickenden A E, Koleske D D and Henry R L 2001 *Electron. Lett.* **37** 1550–1
[44] Neugebauer J and Van de Walle C G 1996 *Festkörperprobleme* **35** 25–43
[45] Tang H, Webb J B, Bardwell J A and Raymond S 2001 *Appl. Phys. Lett.* **78** 757–9
[46] Webb J B, Tang H, Bardwell J A and Coleridge P 2001 *Appl. Phys. Lett.* **78** 3845–7
[47] Wright A F 2002 *J. Appl. Phys.* **92** 2575–85
[48] Seager C H, Wright A F, Yu J and Gotz W 2002 *J. Appl. Phys.* **92** 6553–9
[49] Wolter M, Javorka P, Marso M, Alam A, Carius R, Fox A, Heuken M, Luth H and Kordos P 2001 *Proc. Int. Symp. Electron Devices for Microwave and Optoelectronic Applications* (Piscataway, NJ: IEEE) pp 149–54
[50] Wolter M, Javorka P, Fox A, Marso M, Luth H, Kordos P, Carius R, Alam A and Heuken M 2002 *J. Electron. Mater.* **31** 1321–4
[51] Wolter M, Javorka P, Marso M, Fox A, Carius R, Alam A, Heuken M, Kordos P and Luth H 2002 *Phys. Status Solidi* c **0** 82–5
[52] Lin T Y, Yang H C and Chen Y F 2000 *J. Appl. Phys.* **87** 3404–8
[53] Shur M 1990 *Physics of Semiconductor Devices* (Englewood Cliffs, NJ: Prentice-Hall) p 427
[54] Mittereder J A, Binari S C, Klein P B, Roussos J A, Katzer D S, Storm D F, Koleske D D, Wickenden A E and Henry R L 2003 *Appl. Phys. Lett.* **83** 1650–2
[55] Borgarino M, Menozzi R, Dieci D, Cattani L and Fantini F 2001 *Microelectron. Reliab.* **41** 21–30
[56] Meneghesso G, Haddab Y, Perrino N, Canali C and Zanoni E 1996 *Microelectron. Reliab.* **36** 1895–8